*Transactions*, SMiRT-24
BEXCO, Busan, Korea - August 20-25, 2017
Division VII

# A PROBABILISTIC RISK ASSESSMENT FOR SPENT NUCLEAR FUEL TRANSPORTATION CASKS AFTER LONG-TERM DRY STORAGE CONSIDERING HYDRIDE-RELATED CLADDING EMBRITTLEMENT

**Elmar Eidelpes[1], Luis F. Ibarra[2], Ricardo A. Medina[3]**

[1] Graduate Student, Civil Engineering, University of Utah, U.S.A.
[2] Associate Professor, Civil Engineering, University of Utah, U.S.A.
[3] Associate Professor, Civil Engineering, University of New Hampshire, U.S.A.

## ABSTRACT

This study is part of an investigation into the structural reliability of a spent nuclear fuel (SNF) cask subjected to normal or accidental conditions of transport, after a dry storage period of up to 300 years. A probabilistic approach is chosen for this assessment to account for the uncertainties related to the time-dependent material degradation mechanisms acting on the cask components. Preliminary investigations revealed that the fuel rod cladding is expected to control structural failure of the cask. The probability of failure is likely increased by hydride-related material degradation in the cladding and due to low cladding temperature after long-term storage. Mechanical testing revealed a tendency towards a brittle response on pinching loads at low material temperature of cladding that contains an excessive amount of hydrogen, or after the application of high cladding hoop stresses (CHSs) at high cladding temperatures. Therefore, the hydrogen content ($C_H$) of the cladding and the value of the peak CHS during vacuum drying of the rods were identified as possible controlling parameters of hydride-induced cladding embrittlement. In the scope of the probabilistic risk assessment (PRA), statistical methods are used to predict the expected fuel rod conditions for the moment of transport. This paper presents an exemplary assessment of the probability of hydride-related cladding embrittlement due to high CHSs during vacuum drying or due to excessive hydrogen incorporation in the cladding considering in-reactor corrosion and fission gas release (FGR). The analysis reveals that between 5 and 12% of the SNF rods likely have an offset strain capacity below 2%, and therefore, could react brittle under pinching loads.

## INTRODUCTION

A PRA of the structural integrity of a SNF cask during transportation after long-term storage is being performed, considering storage periods of up to 300 years. Preliminary investigations revealed the high vulnerability of the SNF rod cladding to mechanical loading. Additionally, the cladding is likely affected by material degradation mechanisms during an extended storage period. Thus, the expected fuel rod conditions after long-term storage need to be evaluated to establish a load-bearing capacity for the cladding,

During in-reactor duty of Pressurized Water Reactor (PWR) rods, the high temperature and pressure environment lead to cladding corrosion, and in this process, hydrogen is incorporated in the zirconium alloy (Zircaloy) cladding. After discharge and wet storage of the SNF assemblies, usually a vacuum drying process is performed. During this drying process, the cladding temperature is high, and high CHSs, due to an increased rod internal pressure (RIP), are expected. Recent work presented by Billone et al. (2011, 2012, 2013, 2014), Billone and Burtseva (2016), Chu et al. (2008), and Daum et al. (2006) identified high CHSs at high cladding temperatures as one of the controlling parameters for brittle material behavior of hydrogen containing SNF cladding after the cladding is cooled down. This brittle behavior, specifically observed when pinching loads were applied on the cladding, could be a direct result of hydrides

precipitated in radial direction during cooling. Ring compression tests (RCTs) on irradiated and un-irradiated cladding material showed that, besides other parameters, the value of the peak CHS could play an important role in a hydride related cladding embrittlement. However, some Zircaloy material types, like M5, containing an excessive amount of hydrogen, showed a brittle response that was less dependent on the applied CHS level than on the $C_H$. Billone et al. (2011, 2012, 2013, 2014), and Billone and Burtseva (2016) performed RCT at different material temperatures and introduced a Ductile-to-Brittle-Transition Temperature (DBTT). The DBTT was defined as the minimum temperature that is necessary to obtain 2% offset and 1% permanent strain in the rings, before a significant loading capacity loss (>25%) or stiffness decrease (>50%) of the cladding was detected. The available results in these reports cannot be used to define a precise peak CHS or hydrogen limit as threshold for hydride-related embrittlement; but, typically, a low CHS and a $C_H$ in a moderate range lead to a low DBTT, and ductile cladding behavior can be expected after long-term storage (or at low cladding temperature). Therefore, the assessment of the expected CHS during vacuum drying and the $C_H$ is crucial for a statistical prediction of the rod conditions for the moment of transport.

## METHODOLOGY

A statistical analysis on the expected CHSs in SNF cladding during vacuum drying was presented in Eidelpes et al. (2017). The authors developed two models (Model 1 and 2) based on previous work performed by Rashid et al. (2013). Model 2 is modified in course of the present study to account for FGR and cladding corrosion. The goal is to improve the quality of the results of the statistical likelihood of excessive high CHSs that might lead to a precipitation of hydrides in radial direction, and the identification of rods with an excessively high $C_H$. Based on the RCT results presented in the reports of Billone et al. (2011, 2012, 2013, 2014), and Billone and Burtseva (2016), a peak CHS of 90 MPa is considered as a preliminary lower stress limit, and a $C_H$ of 60 ppm for fuel rods with M5 cladding, and 600 ppm for fuel rods with Zircaloy-4 cladding, is considered excessively high.

### *Modeling of Fuel Rod Conditions*

Several software packages (e.g. SAPHIRE, BISON) predict the fuel rod conditions after a rod is discharged from the reactor. However, these codes require detailed input data that might not be available for a statistically representative set of SNF rods in the U.S inventory. Rashid et al. (2013) developed a model based on the regression of SNF examination data to determine the CHS as a function of the average rod burnup (BU) and the gas temperature. Eidelpes et al. (2017) presented two models to estimate the statistical CHS distribution during vacuum drying. Both Model 1 and 2 use the GC-859 Nuclear Fuel database provided by the U.S. Energy Information Administration (EIA) as input. This database provides information about discharged SNF assemblies in the U.S. from 1968 to 2013. Since the models demand information on fuel rod level rather than information on assembly level, a pseudo rod dataset was created using the number of fuel rods per assembly type as a multiplier for each entry in the database. Only PWR assemblies were considered, and after the rod dataset was generated, 100,000 out of 21 million created entries were randomly sampled to reduce the computational effort for the further statistical analysis of the data. This pseudo rod dataset is considered representative for the U.S. SNF inventory. Both Model 1 and 2 allow an estimation of the RIP during vacuum drying, and consequently, the CHS, for each rod in the dataset as a function of the BU, utilizing the Ideal Gas Law (see Eq. 1) in combination with regression models applied on rod void volume (RVV) examination data and data about the number of gas moles (n) in the rod. To account for the uncertainty in the input, Model 1 and 2 use normally distributed parameter in Eq. 1 for a given BU. The advantages of Model 2 over Model 1 are the consideration of volumetric differences in the rods with respect to assembly type, and a reduced statistical dispersion in the results. In Model 2, a normal distribution was used only for the RVV computation. Rashid et al. (2013) concluded that the number

of gas moles originating from FGR is small compared to the total number of moles in the gas mix of the rod. Eidelpes et al. (2017) performed a limited sensitivity study, showing that the FGR very likely has a low effect on the CHS and argued that, in case of a standard rod, the decreasing RVV with increasing BU is the main controlling parameter for the evolution of the RIP. Therefore, in Model 2, the FGR was neglected and a constant amount of gas in standard rods was assumed. The expected fill gas pressure (between 2.00 and 3.45 MPa) was uniformly allocated to the rods in the inventory. The number of fill gas moles was then calculated using the expected initial RVV with respect to the assembly type.

In the scope of the present study, Model 2 is further developed to consider the effect of FGR and cladding corrosion on the CHS, and to compute the expected $C_H$ in the cladding. This new model is going to be called Model 2b, and the calculated CHS results should be more precise than the results from the previous models. However, the relatively simple computations presented by Rashid et al. (2013) and Eidelpes et al. (2017) are lacking in terms of precision compared to highly complex computer codes, but the goal is to obtain a fuel rod dataset that can be considered representative for the SNF momentarily discharged from the U. S. nuclear power plants (NPPs).

***Discretization of the Ideal Gas Law***

To model the expected fuel rod conditions in the pseudo rod dataset, the rods are discretized in five geometrical subparts (upper and lower plenum; and upper, central and lower active fuel zone), and the Ideal Gas Law is used to calculate the RIP (Eq. 1) (Rashid et al., 2013):

$$\mathrm{RIP} = \frac{\mathrm{nR}}{\sum_i \frac{V_i}{T_i}} \tag{1}$$

The parameter R refers to the Ideal Gas Constant (8.314 4598 $J \cdot K^{-1} \cdot mol^{-1}$), and $V_i$ and $T_i$ denote the void volume ($cm^3$) and temperature (K) of the rod subpart. The parameter n is the number of gas moles of the initial rod pressurization inclusive the number of moles of any additional gas in the RVV released during irradiation of the rod.

***Rod Void Volume (RVV)***

Utilizing the RVV linear regression model, a normally distributed value for the RVV at a specific BU is computed. In Model 2, a mean equal to the expected value of the regression model, and an estimated standard deviation (SD) of 5% of the mean were used to generate a BU-dependent normal distribution for each rod in the dataset. The RVV value was then randomly sampled from this normal distribution to account for the uncertainties in the model. For Model 2b, an additional statistical analysis of the RVV data is conducted. Prediction intervals of the linear RVV regression models are used to better assess the statistical spread. The analysis reveals a SD of approximately 10% of the mean. Consequently, this value is used for the generation of the normal distribution in Model 2b, instead of the original 5%. Therefore, the statistical dispersion in the RVV results is slightly larger than in the Model 2.

The remaining steps in the computational process of Model 2b are the same like in Model 1 and 2. A closed pellet-cladding gap is assumed, and the RVV is allocated to the subparts. Based on the suggestions of Eidelpes et al. (2017), a 1.35-times larger RVV value and a different RVV distribution along the rod axis for rods with Annular Axial Blanket (AAB) fuel pellets compared to rods containing only standard pellets are used in the analysis. The RVV evolution with increasing BU was assumed identical for AAB pellet containing rods and rods containing only standard pellets.

### *Rod Temperature*

Limited data is available on the expected rod temperature during vacuum drying. Thermal examination data measured at different positions in an evacuated dry storage cask during experimental test runs are presented in Dziadosz et al. (1986). Rashid et al. (2013) suggest a linearization of the hottest temperature profile in longitudinal direction of the rod that was obtained with these experiments to calculate the RIP. Eidelpes et al. (2017) used two additional linearization of temperature profiles to account for the assembly position within the cask, based on the work of Dziadosz et al. (1986). The rod temperature profile during vacuum drying for a specific rod in the SNF inventory cannot be directly determined from the available data. However, considering the linearized temperature profiles chosen by Eidelpes et al. (2017) as not overly conservative, the RIP distribution in the dataset can be estimated. For comparison, additional results are obtained assuming a constant rod temperature of 400 C°.

### *Amount of Gas in the Rods*

The remaining unknown parameter in Eq. 1 is the amount of gas in the rods, measured in number of moles n, which is an accumulation of the number of gas moles from the initial rod pressurization, the moles from the FGR, and, in the case of Integral Fuel Burnable Absorber (IFBA) rods, the additional helium mole release originating from the B-10 decay. IFBA rods are characterized by a thin $ZrB_2$ coating of the $UO_2$ pellets. During irradiation, the boron isotope B-10 in the coating decays in a reaction described by Eq. 2 (Monterrosa et al., 2012; Secker and Brown, 2010):

$$B^{10} + n^1 = Li^7 + He^4 \tag{2}$$

The released helium significantly increases the RIP, a phenomenon that is considered in Model 1, 2, and 2b. In Model 2b, the amount of fill gas and eventual additional helium gas in case of IFBA rods (see Eq. 2) is computed in the same way as in Model 2. However, the FGR is considered as well, using a regression model, which is based on available fractional FGR examination data presented in Manzel and Walker (2000), Noirot et al. (2000), and Vesterlund and Corsetti (1994). Figure 1 (a) displays the available data, including the mean, and the 2.5%, 50% (median), and 97.5% quantiles for rods with a BU below 62 GWd/MTU. This value was chosen, since it is the currently permitted BU limit in the U.S. As observed, the FGR increases as the BU increases. Therefore, an exponential curve for the regression of the FGR examination data is chosen. Further, a log-normally distributed value at a specific BU was assumed to account for the uncertainty in the release. For simplicity, a linear regression model was applied on the data in the natural logarithmic domain of the FGR, which is equivalent to the exponential regression in the

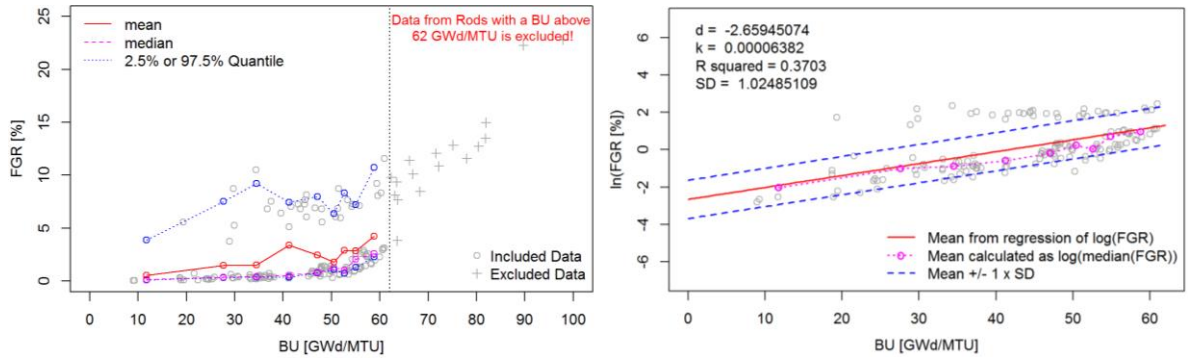


(a) (b)

Figure 1: (a) FGR examination data, incl. statistical parameters, (b) linear regression of ln(FGR [%])

original data domain (see Figure 1 (b)). Consequently, the expected logarithmic distribution to account for the uncertainty in the FGR at a specific BU corresponds to a normal distribution in the logarithmic domain. To determine the FGR in a rod in the database, the BU in combination with the linear regression model is used to compute the mean of the normal distribution. Based on a BU-interval-wise data analysis, a constant, arithmetically averaged SD of 1.0249 is assumed to compute the statistical dispersion. Then, a value is randomly sampled from the generated distribution. The FGR value is computed, using the exponential function, and allocated to the selected rod. Using the information about the fuel mass (kg) and a total amount of available fission gas equal to 31 $cm^3$ per MWd energy yield at 0 °C (Guenther et al., 1988), the number of released fission gas moles can be calculated and added to the gas inventory of the rod. Finally, the RIP can be calculated using Eq. 1 in combination with a constant or a linearized rod temperature profile and under consideration of the expected RVV distribution along the rod axis.

***Cladding Corrosion and Hydrogen Pickup***

Another modification in Model 2b with respect to Model 2 is the consideration of in-reactor cladding corrosion to account for wall thinning and to compute the amount of hydrogen in the material. The oxide thickness (δ) evolution was evaluated specifically for the four major cladding material types commonly used in PWR reactors in the U. S.: Zircaloy-4, ZIRLO, Optimized ZIRLO, and M5, since they show different corrosion behavior. The EIA database does not provide information about the cladding material type of the SNF assemblies in the U. S. inventory. Therefore, a material distribution is established by comparing information provided by Garzarolli and Rudling (2011) about the first-time application of advanced cladding material in U.S. commercial NPPs with the irradiation cycle dates of the assembly and information on assembly vendor that can be found in the database. Figure 2 shows the computed cladding material distribution in the rod dataset. Due to the lack of data, cladding material of all Westinghouse rods that were loaded into a reactor after the year 1991 is considered ZIRLO, whereas the material of the rods loaded into a reactor after the year 2008 is considered Optimized ZIRLO. The cladding material of all Areva rods that were loaded into a reactor after the year 1998 is considered M5.

Foster et al. (2011), Mardon et al. (2010), and Rashid et al. (2006) present corrosion data for the different material types and regression lines for Zircaloy-4, ZIRLO, and Optimized ZIRLO. No data regression is provided for M5 cladding material, and the expected value of δ on M5 cladding for a given BU is estimated from the available data, using a linear function. Similar to the FGR model, the uncertainty in the expected δ for a rod with a given BU is considered by sampling a value randomly from a log-normal distribution. The regression models for the different cladding material types were applied on the data in the natural logarithmic domain. Rashid et al. (2006) present data for the 2.5 and 97.5% quantile of the log-normally distributed, BU-dependent peak δ of Zircaloy-4 cladding, but the available literature does not provide information on the statistical dispersion for a given BU for the remaining cladding material types. For the rods with these materials, the SD of the normal distributions that are used for the δ sampling in the natural logarithmic domain is set equal to the value derived from the available Zircaloy-4 data (0.2489).

The models are presented in Figure 3. In case of Zircaloy-4, ZIRLO, and Optimized ZIRLO, the linear regression of the data in the logarithmic domain corresponds to an exponential development of the expected δ value with increasing BU in the original data domain. In case of the M5 data, the evolution of δ with increasing BU is estimated using a linear function. Therefore, the regression of the data in the logarithmic domain is a logarithmic function. According to Motta et al. (2015), the fuel BU is not a high-

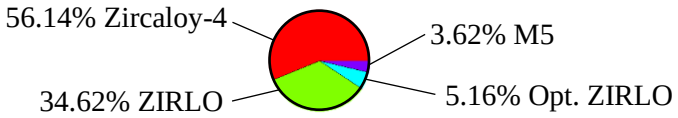


Figure 2: Cladding material distribution in the U.S. SNF inventory.

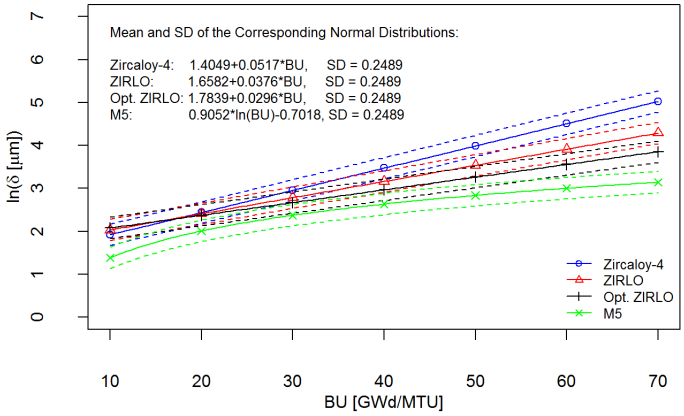


Figure 3: Regression of ln(δ [µm]) for the different cladding material types.

quality parameter to determine the cladding corrosion. However, the results of these models are expected to be adequate for a statistical representation of the cladding corrosion in the U.S. SNF inventory.

Sabol et al. (1994) showed that a typical PWR SNF rod exhibits a thicker oxide layer in the upper zone due to stronger corrosion, which is caused by the higher pressure and temperature in the upper reactor region compare to the lower region. However, Model 2b uses a constant value for δ along the rod axis.

After δ is known, the cladding wall thinning can be computed using the Pilling-Bedworth Ratio ($R_{PB}$) for $ZrO_2$, a factor defining the volumetric expansion of a metallic specimen during corrosion (Eq. 3):

$$R_{PB} = \frac{V_{oxide}}{V_{metal}} = 1.56 \tag{3}$$

where $V_{oxide}$ is the unit volume of the metal oxide after corrosion, and $V_{metal}$ is the corresponding unit volume of the corroded metal before oxidation.

Eidelpes et al. (2017) used an assembly specific Monte-Carlo-Simulation, based on available rod geometry data, to determine the wall thickness and diameter of the cladding. Knowing these parameters, the cladding hoop stress factor (CHSF) and, ultimately, the CHS can be computed (Eq. 4):

$$CHS = \frac{OD-t}{2t} \times RIP = CHSF \times RIP \tag{4}$$

where OD is the outer cladding diameter and t is the cladding wall thickness. The consideration of cladding corrosion leads to a reduction of OD and t in Model 2b, and therefore to higher CHSs during vacuum drying compared to the results of Model 2.

Besides determining the cladding wall thinning, the oxide layer thickness can be used to evaluate the hydrogen concentration in the cladding, using Eq. 5:

$$C_H = \frac{m_H}{m_{Zr}} = \frac{4f}{R_{PB}} \frac{\delta}{(th_{Zr} - \delta/R_{PB})} \frac{M_H}{M_{Zr}} \tag{5}$$

The $C_H$ of the cladding is computed in weight-parts-per-million, δ denotes the oxide thickness, $th_{Zr}$ is the cladding thickness before corrosion, $M_H$ is the molecular mass of hydrogen, and $M_{Zr}$ is the molecular mass of zirconium. Equation 5 is based on a similar formula presented in Courty et al. (2014). The original equation in Courty et al. (2014) uses a value equal to δ to account for the cladding wall thinning; However, in Eq. 5, the volumetric expansion of the oxide layer by a factor of $R_{PB}$ is considered for the determination of the cladding wall thickness after corrosion. The remaining cladding material is assumed thicker than in the formula proposed by Courty et al. (2014), and therefore, the results for the $C_H$ are smaller. The factor f

is the fraction of the available hydrogen that is incorporated in the cladding, and is commonly called hydrogen pickup fraction. It is a material type specific value. Courty et al. (2014) showed that this fraction is not constant during the corrosion process. However, Geelhood and Beyer (2011) suggested the use of a constant pickup fraction for PWR fuel cladding to be utilized in the software package FRAPCON. In the scope of a statistical analysis, a cladding material specific — but constant — pickup fraction seems to be sufficiently precise. Based on the work of Geelhood and Beyer (2011), a pickup fraction of 15.3% for Zircaloy-4, 17.3% for ZIRLO and Optimized ZIRLO, and 10.0% for M5 is selected.

## RESULTS

Figure 4 presents the (a) density, (b) cumulative density function (CDF), and (c) numerical results of the FGR obtained with Model 2b. The terms Low-BU and High-BU refer to rods with a BU below or above 45 GWd/MTU. As observed, the average fractional FGR is 1.78%. The predicted mean for n is 0.03083 mol, which is about 9.2% higher than the value computed with Model 2 (0.02823 mol).

Figure 5 presents (a) a boxplot and (b) the numerical results for the CHSF, categorized in thick cladding tubes (14×14 and 15×15 assembly rods) and thin cladding tubes (16×16, 17×17, and 18×18 assembly rods), including a comparison with the values for hypothetically non-corroded cladding (Model 2). Garzarolli and Garzarolli (2012) suggested these thick and thin cladding categories based on similar OD and t. The cladding wall thinning due to corrosion raises the mean CHSF by about 2.8%, resulting in a relatively small contribution of this parameter to an increased CHS.

Figure 6 presents (a) a boxplot and (b) the numerical results of the $C_H$, sorted by material type. The

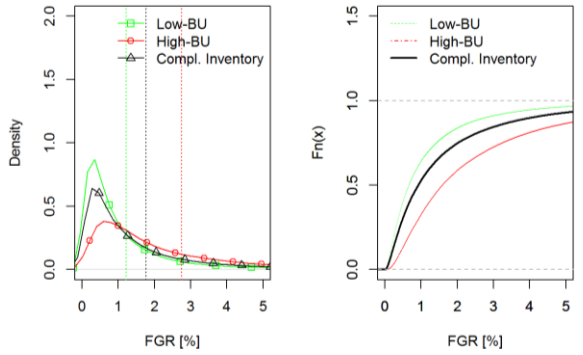


(a) (b)

| FGR [%] | Min | Mean | SD | Max |
|---|---|---|---|---|
| Low-BU | 0.00 | 1.23 | 1.90 | 64.23 |
| High-BU | 0.02 | 2.76 | 3.76 | 100.00 |
| Comp. Inventory | 0.00 | 1.78 | 2.82 | 100.00 |

(c)

Figure 4: FGR obtained for the dataset: (a) density, (b) CDF, and (c) numerical results.

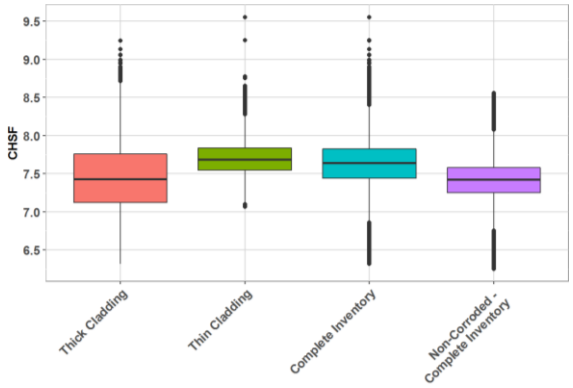


(a)

| CHSF | Min | Mean | SD | Max |
|---|---|---|---|---|
| Thick Cladding | 6.32 | 7.45 | 0.45 | 9.14 |
| Thin Cladding | 7.05 | 7.70 | 0.21 | 9.02 |
| Comp. Inventory | 6.31 | 7.61 | 0.34 | 9.18 |
| Non-Corroded – Comp. Inventory | 6.25 | 7.40 | 0.30 | 8.56 |

(b)

Figure 5: CHSF for corroded and non-corroded cladding: (a) boxplot and (b) numerical results.

horizontal, red lines are the preliminary $C_H$ thresholds (60 ppm for M5 and 600 ppm for Zircaloy-4 cladding) for hydride embrittlement. As can be seen, the $C_H$ exhibits large variations for different cladding types, ranging from an average $C_H$ of 72 ppm for M5 rods, to more than 200 ppm of hydrogen for ZIRLO and Optimized ZIRLO. The mean $C_H$ of ZIRLO rods is almost 20% larger than that of Zircaloy-4, despite the lower oxidation rate. Reasons for this difference are the increased hydrogen pickup (17.3% vs. 15.3%) and the higher average BU (45 GWd/MTU vs. 36 GWd/MTU) of ZIRLO rods compared to Zircaloy-4 rods.

Figure 7 presents (a) a boxplot and (b) the numerical results of the CHS during vacuum drying using linearized rod temperature profiles, including a comparison with the results assuming a constant temperature of 400 C°. The horizontal, red line is the preliminary 90 MPa stress threshold for embrittlement due to radial hydrides. The mean value for the CHS depends strongly on the chosen thermal model and ranges between 17 and 494 MPa. Using the linearized temperature profiles, standard rods experience a mean CHS of 45 MPa. The mean CHS for the IFBA rods is approximately 87 MPa. Considering the complete rod inventory (standard and IFBA rods), the results for the mean CHS are 46 MPa and 67 MPa, assuming linearized temperature profiles and a constant rod temperature of 400 °C respectively. Compared to the results for Model 2 (41 MPa and 60 MPa) presented in Eidelpes et al. (2017), the mean CHSs obtained with Model 2b are approximately 11.4% higher, independently of the chosen temperature profiles.

Using the linearized temperature profiles, approximately 1.71% of all rods experience a CHS above 90 MPa during vacuum drying. About 69% of the M5 rods could have a $C_H$ above 60 ppm. Further, 1.3% of all Zircaloy-4 rods have a $C_H$ above 600 ppm. For the preliminary assessment, these rods are considered

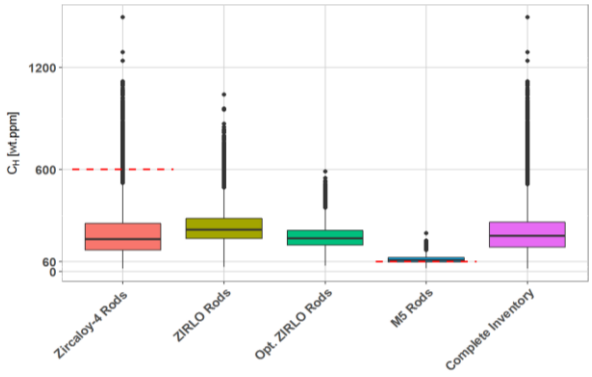


(a)

| $C_H$ [ppm] | Min | Mean | SD | Max |
|---|---|---|---|---|
| Zircaloy-4 | 20 | 220 | 129 | 1657 |
| ZIRLO | 23 | 261 | 96 | 1117 |
| Optimized ZIRLO | 39 | 205 | 70 | 669 |
| M5 | 19 | 72 | 22 | 185 |
| Comp. Inventory | 19 | 228 | 119 | 1657 |

(b)

Figure 6: $C_H$, sorted by cladding material type: (a) boxplot and (b) numerical results.

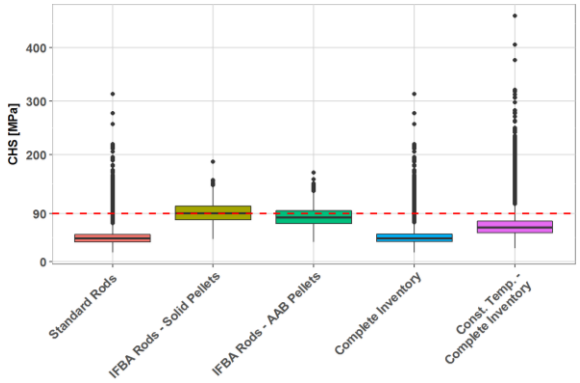


(a)

| CHS [MPa] | Min | Mean | SD | Max |
|---|---|---|---|---|
| Standard Rods | 17.22 | 44.79 | 11.39 | 337.36 |
| IFBA Rods – Solid Pellet | 44.08 | 91.85 | 18.88 | 153.08 |
| IFBA Rods – AAB Pellets | 38.18 | 83.62 | 18.02 | 164.38 |
| Comp. Inventory | 17.22 | 46.09 | 13.77 | 337.36 |
| Comp. Inventory – Const. Temp. | 25.20 | 67.24 | 20.11 | 493.74 |

(b)

Figure 7: CHS assuming linearized temperature profiles, incl. comparison for a constant rod temperature of 400 °C: (a) boxplot and (b) numerical results.

endangered by hydride-related embrittlement when cooled to room temperature. The deformation capacity of these rods under pinching loads is expected to be below the 2% offset and/or 1% permanent strain criterion. The total fraction of the rods in the inventory that exceeds the CHS and/or the $C_H$ threshold is approximately 4.9%. Assuming a constant rod temperature of 400 °C, this fraction increases to 11.7%.

## CONCLUSIONS

This paper extends the work presented by Rashid et al. (2013) and Eidelpes et al. (2017) to assess the probability of hydride-related cladding embrittlement due to high CHSs during vacuum drying or an excessive $C_H$. Model 2b considers the effect of corrosion and FGR in the calculations, and is capable of predicting the hydrogen incorporation into the cladding.

- The mean CHSF is raised due to corrosion by about 2.8% compared to hypothetically non-corroded cladding. Therefore, the effect of cladding corrosion on the CHS can be estimated as small.
- The mean amount of gas that contributes to the RIP is about 9.1% higher when considering FGR.
- The mean CHS computed with Model 2b is 11.4% higher than the value obtained with Model 2.
- Assuming linearized temperature profiles Model 2b predicts that approximately 5% of the rods in the inventory may exceed the preliminary thresholds at which CHS or $C_H$ could lead to brittle cladding behavior under pinching loads.
- Assuming conservatively a constant rod temperature of 400 °C, the fraction of endangered rods raises to 12%

Incidentally, the authors want to emphasize that this analysis is based on preliminary chosen thresholds. Further investigations on the controlling parameters are necessary; e.g., the impact of other variables, like CHS at precipitation temperature, or temperature and CHS evolution during rod cool down.

## ACKNOWLEDGEMENTS

This material is based upon work supported by the Department of Energy Nuclear Energy University Program. Any opinions, findings, conclusions or recommendations expressed in this publication are those of the authors and do not necessarily reflect the views of the Department of Energy.

## REFERENCES

Billone, M. C., and Burtseva, T. A. (2016). *Effects of Lower Drying-Storage Temperature on the Ductility of High-Burnup PWR Cladding*. ANL, Lemont, IL, USA.

Billone, M. C., Burtseva, T. A., Dobrzynski, J. P., McGann, D. P., Byrne, K., Han, Z., and Liu, Y. Y. (2011). *Phase 1 Ring Compression Testing of High-Burnup Cladding*. ANL, Lemont, IL, USA.

Billone, M. C., Burtseva, T. A., Han, Z., and Liu, Y. Y. (2013). *Embrittlement and DBTT of High-Burnup PWR Fuel Cladding Alloys*. ANL, Lemont, IL, USA.

Billone, M. C., Burtseva, T. A., Han, Z., and Liu, Y. Y. (2014). *Effects of Multiple Drying Cycles on High-Burnup PWR Cladding Alloys*. ANL, Lemont, IL, USA.

Billone, M. C., Burtseva, T. A., and Yan, Y. (2012). *Ductile-to-Brittle Transition Temperature for High Burnup Zircaloy-4 and ZIRLO Cladding Alloys Exposed to Simulated Drying-Storage Conditions*. ANL, Lemont, IL, USA.

Chu, H. C., Wu, S. K., and Kuo, R. C. (2008). "Hydride reorientation in Zircaloy-4 cladding." *Journal of Nuclear Materials*, Elsevier B.V., 373(1–3), 319–327.

Courty, O., Motta, A. T., and Hales, J. D. (2014). "Modeling and simulation of hydrogen behavior in Zircaloy-4 fuel cladding." *Journal of Nuclear Materials*, Elsevier B.V., 452(1–3), 311–320.

Daum, R. S., Majumdar, S., Liu, Y., and Billone, M. C. (2006). "Radial-hydride Embrittlement of High-burnup Zircaloy-4 Fuel Cladding." *Journal of Nuclear Science and Technology*, Taylor & Francis, 43(9), 1054–1067.

Dziadosz, D., Moore, E. V., Creer, J. M., McCann, R. A., McKinnon, M. A., Tanner, J. E., Gilbert, E. R., Goodman, R. L., Schoonen, D. H., Jensen, M., and Muellen, C. (1986). *The Castor-V-21 PWR Spent Fuel Storage Cask: Testing and Analyses*. EPRI, Palo Alto, CA, USA.

Eidelpes, E., Ibarra, L. F., and Medina, R. A. (2017). "PRA - Radial Hydride Embrittlement in Spent PWR Nuclear Fuel Cladding." *International High-Level Radioactive Waste Management Conference*, ANS, Charlotte, NC, USA.

Foster, J. P., Colburn, D., Comstock, R., Cook, T., Dahlback, M., Garde, A., Jourdain, P., Kesterson, R., McClarren, M., Svec Nuhfer, D. L., Pan, G., Mundorff, J. P., Yueh, H. K., Bishers, J., File, P., and Boshers, B. (2011). "Zirconium alloys with improved corrosion/creep resistance due to final heat treatments." United States of America, USA.

Garzarolli, F., and Garzarolli, M. (2012). *PWR Zr Alloy Cladding Water Side Corrosion: State of Knowledge on In-PWR Corrosion Analysis Methods of Measured Oxide Data and Oxide Thickness Prediction*. ANT International, Mölnlycke, Sweden.

Garzarolli, F., and Rudling, P. (2011). *Performance Evaluation of New Advanced Zr Alloys for PWRs/VVERS*. ANT International, Mölnlycke, Sweden.

Geelhood, K., and Beyer, C. (2011). "Hydrogen Pickup Models for Zircaloy-2 , Zircaloy-4 , M5™ and Zirlo™." *2011 Water Reactor Fuel Performance Meeting*, CNS, Chengu, China.

Guenther, R. J., Blahnik, D. E., Campbell, T. K., Jenquin, U. P., Mendel, J. E., Thomas, L. E., and Thornhill, C. K. (1988). *Characterization of Spent Fuel Approved Testing Material - ATM-103*. PNL, Richland, WA, USA.

Manzel, R., and Walker, C. T. (2000). "High Burnup Fuel Microstructure and its Effect on Fuel Rod Performance." *Proceedings of the 2000 International Topical Meeting on Light Water Reactor Fuel Performance*, ANS, La Grange Park, IL, USA.

Mardon, J. P., Garner, G. L., and Hoffman, P. B. (2010). "M5® a breaktrough in Zr alloy." *Proceedings of 2010 LWR Fuel Performance/TopFuel/WRFPM*, ANS, Orlando, FL, USA, 577–586.

Monterrosa, A., Iyengar, A., Huynh, A., and Madaan, C. (2012). *Boron Use and Control in PWRs and* FHRs. UCB, Berkley, CA, USA.

Motta, A. T., Adrien, C., and Comstock, R. J. (2015). "Corrosion of Zirconium Alloys Used for Nuclear Fuel Cladding." *Annual Review of Materials Research*, Annual Reviews, 45, 311-343.

Noirot, J., Desgranges, L., and Marimbeau, P. (2000). "Contribution of the Rim to the Overall Fission Gas Release: What do Isotopic Analyses Reveal?" *Fission Gas Behavior in Water Reactor Fuels Seminar*, NEA, Cadarache, France, 223–234.

Rashid, J., Dunham, B., Zhang, Y., and Montgomery, R. (2006). *Spent Fuel Transportation Applications: Longitudinal Tearing Resulting from Transportation Accidents - A Probabilistic Treatment*. EPRI, Palo Alto, CA, USA.

Rashid, Y. R., Sunderland, D. J., Lyon, W. F., and Kubischta, K. E. (2013). *End-of-Life Rod Internal Pressures in Spent Pressurized Water Reactor Fuel*. EPRI, Palo Alto, CA, USA.

Sabol, G. P., Comstock, R. J., Weiner, R. A., Larouere, P., and Stanutz, R. N. (1994). "In-Recator Corrosion Performance of ZIRLO™ and Zircaloy-4." *Zirconium in the Nuclear Industry: Tenth International Symposium, ASTM STP 1295*, Garde A. M., Bradley E. R., Philadelphia, PA, USA, 724–744.

Secker, J. R., and Brown, J. A. (2010). "Westinghouse PWR Burnable Absorber Evolution and Usage Westinghouse PWR Burnable Absorbers." *2010 ANS Winter Meeting and Nuclear Technology Expo*, ANS, Las Vegas, NV, USA, 1–16.

Vesterlund, G., and Corsetti, L. V. (1994). "Recent AAB Fuel Design And Performance Experience." *Proceedings of the 1994 International Topical Meeting on Light Water Reactor Fuel Performance*, ANS, West Palm Beach, FL, 62–70.